LRP 491/94

February 1994

COAXIAL PLASMA GUN IN THE HIGH DENSITY REGIME AND INJECTION INTO A HELICAL FIELD

S. Schaer

C R P P

ÉCOLE POLYTECHNIQUE FÉDÉRALE DE LAUSANNE - SUISSE

LRP 491/94 February 1994

COAXIAL PLASMA GUN IN THE HIGH DENSITY REGIME AND INJECTION INTO A HELICAL FIELD

S. Schaer

LRP 491/94 February 1994

COAXIAL PLASMA GUN IN THE HIGH DENSITY REGIME AND INJECTION INTO A HELICAL FIELD

by S. Schaer

ERRATA

Formula (27) at the bottom of page 8 should be:

$$l_i = \frac{\int_0^a \left(B_{\theta 0}^2/2\mu_0\right) 2\pi r dr}{\left(B_{\theta 0,a}^2/2\mu_0\right)\pi a^2} \cong 1.2 \qquad (27)$$

COAXIAL PLASMA GUN IN THE HIGH DENSITY REGIME AND INJECTION INTO A HELICAL FIELD

SAMUEL F. SCHAER

Centre de Recherches en Physique des Plasmas,
Association Euratom-Confédération Suisse,
Ecole Polytechnique Fédérale de Lausanne, 21 Av. des Bains,
CH - 1007 Lausanne, Switzerland

Secondary School Student at:
Gymnasium,
Kantonsschule Hardwald,
CH - 4600 Olten, Switzerland

ABSTRACT: A modified coaxial gun in the high density regime of 20-70 mT of He restgas, i.e. without a fast-acting valve gaspuff, energized by a 1200J HV sinusoidally damped capacitor discharge with peak currents of 86kA in the potential range of 10-15 kV, was investigated. The acceleration of the current sheet inside the gun was studied, and an MHD current element model derived, which is in very good agreement with experimental data. The model suggests that thermal diffusion can be neglected during the acceleration phase and furthermore explains in a very simple way the sheet velocity limitation. At the muzzle of the gun, the plasma is magnetized by inducing a toroidal current in it (6.5 kA) through a permanent radial field (.2T), generating a confining poloidal field. The injection of the generated current-carrying plasmatorus into the driftspace was studied by means of a diamagnetical probe array, for two different cases: (1) toroidal bias field, and (2) helical bias field. The inner electrode, which has negative polarity to begin with, is continued into the driftspace by a considerably thinner, pyrex insulated central conductor, generating the toroidal bias. Quasi-Tokamak geometry is reached in the helical case ($q\cong3, \beta_p\cong.7, l_i\cong1.2$). The necessary axial bias field strength was thereupon calculated according to Tokamak-equilibrium (axial bias field coil discharge: aperiodically damped, flywheel diode, max. field strength .26T). Second half-period breakdown was observed, thus a positive electrode was present most of the time. This is a unique way to achieve autopreionisation. Plasma gun operation is very much breakdown dependent, specially in the region of the muzzle. This problem made it necessary to construct a special compensation coil for the axial field coil. The mean torus speed in the driftspace was 2 2 cm/µsec. The tori were azimuthally very homogenous and exhibited enhanced stability. Transverse expansion at ejection and in the driftspace is prevented by a unique rarefaction wave-pattern resulting from the Mach 50 supersonic flow. The toroidal current was observed to decay continuously, not abruptly. No n type or oscillarotry instabilities were encountered. These findings are important for future designs of guns where a stable and homogenous torus is needed, such as magnetic confinement injectors (for Spheromaks,etc.).

1. INTRODUCTION

Plasma guns were first investigated by J. Marshall and H. Alfvén between 1958 and 1960 [1-4]. Most studies concerning this particular device were done between 1960 and 1965 [5-10]. Plasma guns were thoroughly investigated; however, a lot of questions remained unanswered, especially if the gun is operated in the high density regime. Thus the investigation of gun phenomena is still today a research task [11-14]. The field of applications is very large: Plasma guns are used to inject plasma into all kinds of magnetic confinement devices, i.e. into conventional mirror machines [15], cusped traps [16], tandem mirrors [17], octupoles [18], Tokamaks [19], Stellarators [20], and Spheromaks [21]. Furthermore, they are important to plasma dynamics research (MHD and kinetic) [22], dynamics of fast ionizing shock waves in MAST[1] devices [23], and for space propulsion [24]. Plasma centrifuges [25] are based on coaxial guns. Finally, they are used for deposition processes [26] and for REB[2] - interaction studies [27]. A closely related field, i.e. dense plasma foci [28], has also become of considerable interest. It is thus of great interest and value to achieve an understanding of plasma gun phenomena. This paper wants to make its contributions towards achieving that goal.

In section 2, the theory of plasma guns in the high density regime is descibed qualitatively, then quantitatively by an MHD current element model with analytical solutions for the sheet structure and speed derived by the author. The formula of the current induced in the plasma through flux conservation is discussed, as the processes in the driftspace and Tokamak equilibrium. The parameters of the plasma encountered in this particular design are given. In section 3, the experimental apparatus and design considerations are presented. That section is mainly technical, since unanticipated "design-effects" are presented in section 4, which also presents the results of the diamagnetic and magnetic diagnostics and shows the very good agreement with the mathematical model. The measurement of the magnetized plasma and of the preceding fast shock wave is described. In addition, the discharge current diagnostics by means of Rogowski belts are given. The paper concludes with section 5. For the notation of the formulae the reader is referred to the appendix. The figures are found at the end of the report, where the figure-text is given in the "figure captions" section.

---

[1] Magnetic Annular Shock Tube = Coaxial Plasma Gun

[2] Relativistic Electron Beam

2. THEORETICAL CONSIDERATIONS

The model that one has to apply to a particular plasma gun is heavily dependent on the design parameters, i.e. capacitor bank characteristics, aspect ratio of the gun, whether or not the gun is operated with a gaspuff, the kind of gas used, etc. Thus for the assumptions, approximations and computations, the design parameters have been introduced from section 3 & 4.

2.1. Qualitative Description

A capacitor discharge takes place between 2 coaxial cylinders. Because of the lowest circuit self-inductance and an ignition aid mounted on the inner electrode, breakdown occurs at the rear end of the gun (breech), where the energy is supplied. Thus a homogenous plasma disc forms, which is accelerated as current sheet towards the other end of the gun (muzzle) due to the magnetic pressure generated by the toroidal field of the dircharge current. The sheet acts as a snowplow, having to pull the rest gas. Thus a region of increased density forms in front of the sheet, whereas behind the sheet the density is very low. The front of the increased density region propagates as a high Mach number shock wave with sufficient energy for partial ionization. The plasmoid (current sheet) starts to rotate around the axis during acceleration, due to a resulting Lorentz force. These processes are illustrated in Fig. 1. When the toroidal plasmoid reaches the other end, it passes a permanent radial field, and through flux conservation a toroidal current is induced in it generating a confining poloidal field (Fig. 2). Finally, the plasmoid is ejected into the driftspace. A large current would be interrupted by this ejection, thus a high voltage would be induced and would fire a second plasma. But this voltage spike is suppressed by means of a thin, insulated central conductor fixed at the end of the inner electrode. The leakage current through the central conductor[3] for its part generates a toroidal field; Tokamak field geometry is reached upon the addition of a third field, the coil-generated axial bias. This configuration is very similar to half a small spheromak, since the toroidal plasmoids generated by the gun are elongated and thus compact (Fig. 3). Now the toroidal current in the plasma is measured as it propagates down the driftspace. It has to be mentioned that plasma can very well propagate after extinction of the toroidal current in it. This is the broad outline of what happens in this experiment. The following sections describe these phenomena mathematically and in greater detail.

2.2. Model for the Acceleration Phase

The classical snowplow model [29] is very well applicable to this gun, because (1) there is preionisation, (2) the sheet speed < thermal speed, and (3) collisions between particles are important, since the gun is operated in the high density regime. The plasma sheet is very homogenous due to a clean, homogenous breakdown and because azimuthal exchange is fast, since the thermal speed < Alfvén speed. Wall friction due to ion drag ocurrs at much higher speeds than encountered in this experiment, thus it is neglected (especially for helium the drag is negligible, but not for argon [30]). The ion current is negligible too, since again the density is high, so that there are well enough ions in the central region hitting the cathode to strike out electrons. This is important because the electric field across the plasma is very small after breakdown, so that electrons are only able to leave the cathode through a collision interaction. According to the plasma parameters and previous papers , Maxwellian distribution is assumed for the electrons with a mean temperature of 10 eV. That value was confirmed by previous authors by means of magnetoacoustic oscillations and inference of plasma parameters from other measurements [6,7,31]. Since the design parameters of this gun are in the same

[3] The central conductor leakage current will be discussed in section 4

range, the electron temperature was not measured again; it would be beyond the scope of this work. 10 eV is well below the occurrence of run-away electrons [32]. Table 1 gives the parameters of the plasma (the design parameters have been introduced into the computations):

Table1: Plasma parameters

Electron Temperature	10 eV
Mass Density of the He Restgas (optimum)	$1.1 * 10^{-5}$ kg m^{-3}
Mean Free Time	1.9 ns
Mean Free Path	4.3 mm
Degree of Ionisation (Saha)	100%
Plasma Conductivity for I ⊥ B	$3.2 * 10^{4}$ S
Max. Magn. Field of Discharge Current	.4 T
Mean Electron Larmor Gyration Freq. at Max. of Magn. Field	15 Ghz
Mean Electron Larmor Gyration Radius	$3.3 * 10^{-5}$ m
Hall Parameter	174 (>>1)
Debye Length	$5.8 * 10^{-7}$ m
Number of Particles in Debye Sphere	$1.34 * 10^{3}$
Voltage across Plasma at Discharge Current Max.	25 V

For the mean free time, the mean free path, and the conductivity computation the Spitzer relations [33] have been used. A Laplace network analysis was carried out for the discharge current, but is not shown here. From the analysis it was seen that to assume a current of the form $I = I_0 \sin\omega t$ (1), where I_0 is the amplidude of the ignition half-period, within which the plasma is ejected (in this case, only that very period is of interest), is very reasonable, since also $L_{circuit} >> L_{gun}$, and dL_{gun}/dz is very small, i.e. ω remains essentially constant. According to table 1, the discharge current is fully thermalized. The transverse electron driftspeed including the larmor gyration correction factor is given by:

$$V_d = \frac{I_0 \sin\omega t}{4\pi r n e \sqrt{2Dt}} \qquad (2)$$

$$D = \frac{1}{\mu_0 \sigma}; \quad \sigma = 14.86 \frac{\pi \varepsilon_0 (kT)^{3/2}}{Z m_e^{1/2} e^2 \ln\Lambda}; \quad \Lambda = \frac{12\pi(\varepsilon_0 kT)^{3/2}}{n^{1/2} e^3} \qquad (3,4,5)$$

The infinitesimal elements (concentric rings) are therefore treated as magneto-hydrodynamical current elements. Compare with fig. 4 & 5; from momentum considerations, it is readily found that:

$$\left| \frac{d}{dt}[Mu_z] = I_0^2 \sin^2\omega t \cos\alpha \frac{\mu_0 \Delta r}{4\pi r} \right| \qquad (6)$$

$$\left| \frac{d}{dt}[Mu_r] = I_0^2 \sin^2\omega t \sin\alpha \frac{\mu_0 \Delta r}{4\pi r} \right| \qquad (7)$$

B has to be averaged over the sheet lenght because of ∇I_{axial}. The factors $\sin\alpha$ and $\cos\alpha$ appear because of $\nabla u_{z,radial}$ and because the discharge current is confined within the curved sheet. M is the total mass, i.e. the mass of the hot current sheet region expanding according to $(2Dt)^{1/2}$, and the snowplowed mass by the sheet. In the high density regime, snowplowing is both caused by collisions and by collisionless Coulomb turbulence, so that ξ is essentially 1; therefore it will not be

written in the following formulae. From the shock wave theory of Hugoniot-Rankine [34], where it is implemented that the Mach number $N_m >> 1$:

$$\mu^2 = \frac{\gamma-1}{\gamma+1} = \frac{1}{f+1};\quad u_s = \frac{u_z}{1-\mu^2} = \frac{f+1}{f} u_z;\quad p_1 = \frac{f+1}{f} u_z^2 \rho_0 \qquad (8,9,10)$$

Upon calculating the total mass as discussed above and performing a couple simple manipulations, (6,7) turn into:

$$M = 2\pi r \Delta r (1+f)\rho_0 \left(\sqrt{2Dt} + \frac{1}{f} \int_0^t u\,dt \right) \qquad (11)$$

$$\left| \frac{d}{dt}\left(r \frac{dz}{dt}\left(\sqrt{2Dt} + \frac{1}{f}\int_0^t u\,dt \right)\right) = I_0^2 \sin^2\omega t \cos\alpha \frac{\mu_0}{8\pi^2 r (1+f)\rho_0} \right. \qquad (12)$$

$$\left. \frac{d}{dt}\left(\frac{d(r^2)}{dt}\left(\sqrt{2Dt} + \frac{1}{f}\int_0^t u\,dt \right)\right) = I_0^2 \sin^2\omega t \sin\alpha \frac{\mu_0}{4\pi^2 r (1+f)\rho_0} \right| \qquad (13)$$

The boundary conditions of the system (12,13) are clear, for t=0 they are: dz/dt=0, dr/dt=0, z=0, $r=r_0$, $\cos\alpha=1$, $\sin\alpha=0$. Radial motion and electrode wall reflections[4] only have a small impact on the current sheet front and therefore on u_z. Disruptions or discontinuities in the sheet are quickly compensated with new ionized gas. However, the snowplowing is affected since it is no longer parallel to the axis. In the following, axial snowplowing only will be assumed for simplicity, and a posteriori it will be seen that the error introduced is negligible. Thus dr/dt is neglected, but (12,13) used for numerical integration in order to obtain a mean value for $\cos\alpha$[5]. Then the system of (12,13) reduces to:

$$\frac{d}{dt}\left(\frac{dz}{dt}\sqrt{2Dt} + \frac{1}{2f}\frac{d(z^2)}{dt} \right) = I_0^2 \sin^2\omega t \frac{\mu_0 \cos\alpha}{8\pi^2 r^2 (1+f)\rho_0} \qquad (14)$$

which is a second-order unlinear, inhomogenous differential equation with particular solutions for special coefficients, if it is analytically solvable at all. An analytical solution can be obtained upon assuming $(2Dt)^{1/2} = \langle d \rangle$ to be constant, as previous authors have observed it [31]. The term with $d(z^2)/dt$ is dominant, so that diffusion only plays a minor role and could be neglected; the snowplowed shock mass is >> than the sheet mass. This is confirmed upon numerical integration of (14), both for constant and time-varying diffusion length. For completeness however, <d> is included in the following formulae[6]. The equation is then easily solved by separation of variables and analytical solutions for z and u_z dependent on time and the parameters are obtained:

---

[4] The impact is an amplification of the density gradient within the sheet.

[5] The author does not want to focus in on the numerical integration, because the following analytical formulae give the same values for u_z with negligible relative error.

[6] In section 2.4 <d> will have to included in the consideration. Generally, for larger t, <d> has to be included, so that it is also included in the following formulae.

$$K = \frac{\mu_0 \cos\alpha}{8\pi^2 r^2 (1+f) p_0} \tag{15}$$

$$z = \frac{-\langle d\rangle + \sqrt{\langle d\rangle^2 + \frac{1}{2f} K I_0^2 \frac{1}{\omega^2}(\omega^2 t^2 - \sin^2\omega t)}}{\frac{1}{f}} \tag{16}$$

$$u_z = -\frac{K I_0^2 (\omega t - \sin\omega t \cos\omega t)}{2\omega \sqrt{\langle d\rangle^2 + \frac{1}{2f} K I_0^2 \frac{1}{\omega^2}(\omega^2 t^2 - \sin^2\omega t)}} \tag{17}$$

[6] found similar formulae, except K was different since no snowplowing was included, because the gun was operated in the "slug" gaspuff mode with acceleration of plasma into vacuum. Furthermore, the equation did not include <d>, thus the from is slightly differnt; the double integration of $\sin^2\omega t$ however remains the same as in this case. From the numerical integration the mean value of $\cos\alpha$[7] is computed to ≅ 1/2 (the sheet becomes conical). Table 2 gives some sample values for different times at the mean radius of 4 cm, computed according to (16,17), where the optimum parameters have been introduced from section 4; <d> is computed to have an av. value of 1 cm according to table 1 and (4) in the case of $(2Dt)^{1/2}$. The mean radius of 4 cm was chosen, because the toroidal plasma current density has a maximum there, and the toroidal current is what was measured by the diamagnetical probes[8].

Table 2: Sample values of z and u_z for different t at r=4 cm

t (in μsec)	z (in cm)	u_z (in cm/μsec)
1	0.25	0.9
2	2.5	3.5
3	6.6	4.5
4	11	4.2
5	15	3.5

If <d> were set zero in (16,17), the relative error of u_z within the relevant times of table 2 would be less than 2%. Therefore, thermal diffusion does not have to be considered for the relevant times during the acceleration phase in this experiment and most other plasma guns, where the ejection time might be even shorter. Fig. 6 & 7 show the graphs of z(t) and $u_z(t)$; z(t) is very quickly close to be linear, thus a plasma gun in the high density regime will exhibit velocity limitation, as observed by previous authors [35]. If the functions are evaluated over such a long time, damping should be included, since the current can no longer be assumed to be oscillatory in that case. However, this only gives smaller values of the functions at larger t, the limitation in the oscillatory case is not affected. And again, further periods are of no interest in this experiment, since the sheet is ejected within the first half-period. Fig. 8 shows the motion of the current sheet during acceleration computed according to (16,17). The front surface is hyperbolical; this figure is in very good agreement with image converter photographs of previous authors [5,7,11]. Of course, this model cannot account for all effects. For example, the spin of the torus was neglected, thermal diffusion taken constant, no electron nor ion temperature gradient was included, axial snowplowing only was considered, electrode material ablation

[7] This factor too was assumed to be constant during acceleration

[8] The two INOX-cylindrical electrodes of the discharge chamber have the radii 3 cm and 5 cm

neglected, etc. . But to account for everything is widely beyond the scope of this work and the necessity of having to include them for experimental testing of the model (16,17). In section 4 it will be seen that the values of table 2 are in very good agreement with experimental data.

2.3. Ejection Phase at the Muzzle of the Gun

When the plasmoid reaches the muzzle, it is ejected from the gun due to high u_z (Fig. 2). It is not exactly known, when the discharge current through the sheet is interrupted. One might expect that the current continues to flow as an arc between the edges of the two cylinders, until finally it is interrupted. But experimental data suggest that the gun remains short circuited at the muzzle, so that the sheet can exit freely. The central part of the sheet in the driftspace is therefore heavily dependent on the aspect ratio of the gun. For small aspect ratio, it will be flattened [11], but for a large one very conical [7]. These processes are extraordinarily complicated to calcualte, a very complex simulation would be involved, giving just conclusions about processes of second priority. (18) gives the toroidal current induced in the plasma, where for the flux conservation it has been assumed that the flux in the driftspace be enclosed totally within the outter aluminum cage (section 3). Ξ is a geometry dependent factor, whereas κ has to be assumed (1 in our case).

$$I_p = \frac{\kappa \Phi}{\mu_0 \Xi} \; ; \quad \Xi = \left(b - \frac{2}{3} a + R \left(\frac{1}{2} + \ln \frac{b}{a} \right) \right) \tag{18,19}$$

This current magnetizes the plasma producing a confining poloidal field, which drastically aids the stability of the ejected plasma rings. These rings really do have enough mass to be considered as such, since thermal diffusion should not be forgotten. The current is then distributed over the whole torus cross-section with a gradient. At the ejection, a highly supersonic flow of Mach 50 enters a region of lower pressure. There are two edges at the muzzle, one of the inner and one of the outter cylindrical electrode. Fig. 9 shows the rarefaction wave pattern that forms [34]. It is readily seen that this prevents transverse expansion at first, therefore enhancing stability. An exact computation of the intercepting shock wave pattern, which is quite complicated since the plasma also rotates and magnetic fields are involved, would be widely beyond the scope of this work.

2.4 Driftspace Phase without Axial Bias Field/ >> Toroidal Bias

Without axial bias field means with toroidal bias only, since the helical bias will be generated by a superposed axial field to the toroidal field. The phenomena at ejection are very complex: Bohm diffusion, curvature drift, rarefaction wave pattern, rotation around the axis, poloidal field envelopping, X-point occurrence, etc. . A simple approach from momentum conservation is made in the following, where radial motion and transverse expansion are neglected to begin with (rarefaction waves prevent transverse expansion). From momentum conservation:

$$u_0 \left(\sqrt{2Dt_0} + \frac{l_{gun}}{f} \right) = \frac{1}{2f} \frac{d(z^2)}{dt} + \left(\sqrt{2D(t + t_0)} + \frac{l_{gun}}{f} \right) \frac{dz}{dt} \tag{20}$$

$$z = \frac{-A + \sqrt{A \left(A + \frac{2u_0 t}{f} \right)}}{1/f} \tag{21}$$

$$u_z = \frac{u_0 \sqrt{A}}{\sqrt{A + \frac{2u_0 t}{f}}} \qquad (22)$$

Where $A=(<d>+l_{gun}/f)$; t and z are set zero at the time of ejection. The same approximations have been made to solve (20) as to solve (16). <d> has to be considered in this case at larger t, otherwise the induced error is of the order of 8%. Table 3 shows some sample values for u_z in the driftspace, and fig. 10 & 11 show the graphs of z(t) and $u_z(t)$ for the plasmoid in the driftspace.

Table 3: Sample values of u_z in the driftspace for different t (t=0 at ejection) at r=4 cm

t (in μsec)	u_z (in cm/μsec)
1	3.0
2	2.6
3	2.4
4	2.2
5	2.0
6	1.9

The speed that is finally measured in the form of a time delay is that at the mean radius (4 cm), since the toroidal plasma current density has got a maximum there.

2.5. Driftspace Phase with Axial Bias Field/ >> Helical Bias

In that case, the magnetized elongated torus is injected into a helical bias field, produced by the toroidal field of the leakage current in the central conductor and the coil-generated field. The plasmoid moves as in section 2.4, but it is slowed down slightly by the magnetic pressure gradient of the bias field. In that way, Tokamak geometry is reached. Recent findings at the Spheromak SPHEX with an independent central iron rod [21] show an enhancement of torus stability. In this work it was tried wheather it was possible to use an elongated central electrode (as described) instead of an independent rod in order to achieve better gun operation and enhanced stability after injection. This will be discussed in section 4. The necessary axial field strength has been computed according to Shafranov's formula (23) [36,37], which has been derived for Tokamak equilibria:

$$B_a = -\frac{\mu_0 I_p}{4\pi R}\left(\ln\frac{8R}{a} + \Gamma - \frac{1}{2}\right); \quad \Gamma = \beta_p + \frac{l_i}{2} - 1 \qquad (23,24)$$

The definitions used for l_i, β_p, and q are:

$$q = \frac{1}{2\pi}\oint \frac{1}{R}\frac{B_\Phi}{B_\theta} \cong \frac{aB_\Phi}{RB_\theta} \cong 3 \qquad (25)$$

$$\beta_p = 1 + \frac{1}{(aB_{\theta,a})^2}\int_0^a \frac{dB_\Phi^2}{dr} r^2\, dr = 0.7 \qquad (26)$$

$$l_i = \frac{\int_0^a \left(B\theta_0^2/2\mu_0\right) 2\pi r dr}{\left(B\theta_{0,a}/2\mu_0\right)\pi a^2} = 1.2 \qquad (27)$$

The numerical values are given for the optimum parameters from section 4. The field profile inside the torus was taken to have a squared parabolical form. Effects of that field computed according to Tokamak equilibrium were studied and are presented in section 4.

3. EXPERIMENTAL APPARATUS

Due to the unique design of the gun, some effects not anticipated were found. These are discussed at the beginning of section 4, here, only the apparatus itself is presented as it has been planned.

3.1. Modified Coaxial Gun and Driftspace

Fig. 12 shows the heartpiece of the apparatus. The reader is also referred to photographs 1-3. The discharge chamber lies between r = 3 cm and r = 5 cm, having a total acceleration length of 15 cm. The electrode material is INOX, the insulator teflon. Actually, the discharge is short circuited, by the central conductor (insulated from the driftspace by a thin pyrex tube), the copper cross, the bottom plate, and the outter aluminum cage. But due to the high self-inductance of that circuit, the discharge takes place anyway. The leakage current through the central conductor generates the toroidal field necessary for the helical bias, together with the axial field coil. Due to the central conductor, the large discharge current is not interrupted, when the plasmoid is ejected. In previous experiments, the current has been observed to continue as a helical pinch, if this is not provided [7]. The pyrex tube of the drift space has an inner radius of 8.5 cm and a total lenght of 48 cm. The diagnostics and the axial field coil are held by a hexagonal cage, embedded between the aluminum cage and the pyrex tube. The radial field at the muzzle of the gun is generated by assembled permanent-magnet cubes, liing on top of the inner electrode. The flux is guided to the muzzle through the massive iron plates (not in axial symmetry) and the central iron core. The permanent field strength reached in this manner is 0.2 T. The leakage flux is negligible. Unique are the central conductor and the outer aluminum cage. At the gun breech, an INOX ring with a sharp edge has been mounted on the inner electrode to stimulate ignition. The polarity has been chosen negativ to begin with. In section 4 it is explained, why the polarity was not changed although it was found that a positive inner electrode stimulates immediate breakdown. For more details, the reader is referred to the legend of Fig. 12.

3.2. Vacuum System

Helium was chosen as the working gas; the pressure was varied between 20 mT and 70 mT. For this pressure range, a common rotary pump is adequate. The vacuum chamber is evacuated well below 1 mT, before helium is admitted. This experiment does not use a fast-acting valve as a gaspuff, thus the helium is admitted through a manual valve. After a period of preliminary tests, it was found that the discharge chamber, especially the teflon insulator, became too dirty due to the oil steam coming from the pump. Therefore, a liquid nitrogen cryotrap has been added and the problem was reduced to a very well acceptable level.

3.3. Main and Vertical Field Coil Discharge System

The triggering is performed by the same chain of pulse amplifiers for both discharges: A manual switch triggers a TTL time base unit with a resolution of 1 µsec, from where everything else is triggered, i.e. discharges, oscilloscopes, etc. The timed pulse for each discharge is amplified from -5V to +300V, then from +300V to -5kV by a thyratron pulser. That pulse is then coupled into a diode safety electronic by a HV coupling-transformer. Finally the ignitron is fired discharging the capacitors. The data given below have been calculated using transient Laplace network analysis, and are in agreement with experimental data.

Main Discharge

The potential on a 13.7 μF low-inductivity capacitor is varied between 9 kV and 15 kV for the different shots. For 15 kV, the charging time is approx. 3 min. The discharge current has the form of a damped sinusoid, with τ_{plasma} = 15 μsec and f_{plasma} = 200 kHz when a plasma is ignited, and $\tau_{central}$ = 55 μsec / $f_{central}$ = 100 kHz when the current flows through the central conductor. Originally, the circuit was intended to give a plasma discharge current of 100 kA, but due to second half-period breakdown discussed in section 4, the maximum plasma discharge current is 86 kA. To keep the inductivity of the circuit low, the energy is transported from the capacitor to the gun by a low-inductivity slab line.

Axial Field Coil Discharge

Two electrolytic capacitors having a total capacity of 6200 μF are charged to a potential of 50 V to 400 V, which is varied as a parameter. The polarity of the field generated by a coil of 25 turns can be changed by exchanging the cables. Coil currents reached are between 500 A and 4000 A, according to the discharge potential. The discharge itself is aperiodically damped by means of a flywheel diode, where t_{rise} = .7 msec and τ = 2 msec. The charging time is 4 min for 400 V. The maximum field strength in the middle of the coil is 0.26 T.

3.4. Diagnostics

The discharge currents are measured by Rogowski coils; i.e. one for the total discharge current, one for the current through the central conductor, and finally one for the axial field coil discharge. For plasma diagnostics, an array of 9 diamagnetical probes held by the hexagonal cage around the quartz tube is used. These probes are at a certain distance apart from each other; the time delay is measured and thus the velocity obtained. What is actually measured by the probes is the time-derivative of the flux generated by the toroidal current in the plasma. The signal is integrated by a passive RC-network, then directly registered by a digital storage oscilloscope. Each probe consists of two nested loops with different radii, hooked up in such a manner that only the flux through the area between the two loops is measured in dependence of time. This procedure minimizes noise and the signal is not affected during the flat-top of the bias field. Fig. 13 shows the array of probes and one probe in detail. The maximum of the signal also allows the computation of the toroidal current. In this case, the computations were rather complex, since the torus is moving. The formula found is so much geometry dependent, that it is not discussed here. Fig. 13 also shows 3 planes with 3 magnetical coils each. Each coil consists of 12 windings. With that second array the uniformity of the toroidal current can very easily be measured. Instabilities up to n=3 are possible to be detected. Again, the signals are integrated by a passive RC-network and registered by a digital storage oscilloscope. For some shots with marginal parameters, it was necessary to feed the signal into a filter first, in order to reduce RF-noise.

4. RESULTS

First, some results that affect the design of a coaxial plasma gun are going to be presented. Then, in the second part, the actual results of the diagnostics will be presented.

4.1. Effects of Electrode Polarity : Second Half-Period Breakdown

This consideration starts at the time, where the ignitron of the main discharge has been fired. The energy is delivered to the gun, the central cylindrical electrode having negative polarity. The inductivity of the short-circuit through the central conductor and the aluminum cage is much higher (4 times) than the discharge inductivity, so that one expects a breakdown. The electric field between the electrodes is still high, so that electrons can leave the central electrode. Now, the magnetic field of the current flowing through the central electrode (because the discharge current starts to flow) exerts a force on the electrons deflecting them in the axial direction (also, the restgas is not preionized at that timepoint). That field is strong enough, so that the electrons cannot reach the outer, positive cylindrical electrode. Thus breakdown does not occur, and the current flows through the central conductor. But when the second half-period of the potential is reached, i.e. the outer cylinder is negative and the inner positive, electrons leave the outer cylinder and first are in a region of weaker toroidal magnetic field[9]. They have gained enough transverse velocity when entering the strong field region close to the inner cylinder, thus they can reach it and breakdown occurs. This is also enhanced by the preionisation taking place on the first breakdown effort. Without a central conductor continuation, breakdown has to take place on the frist have-period. But the polarity should still be negative to begin with in the central conductor operation mode, because autopreionisation is very conveniently performed, resulting in very homogenous, clean breakdowns on the second half-period. Note that the central conductor does not loose its original purpose to generate a toroidal field in the driftspace: When the plasma is ignited, the current in the central conductor circuit loop decays due to the high inductivity with $\tau = 55$ µsec, but the plasma is ejected within 3 µsec to 4 µsec, so that the toroidal field is still well maintained! Fig. 14 shows a typical oscillogram for the total discharge current and the current through the central conductor. Note that the gun remains short circuited after breakdown.

4.2. Sensitivity of the Breakdown to Magnetic Field Components

This problem was first encountered when the operation of the axial field coil was started. Whenever there was a helical bias instead of a toroidal, no signal was measured by the diamagnetical probes. This can only suggest one thing: there is no toroidal current leaving the gun. It was found that this is due to a stable electron orbit effect at the muzzle of the gun. A complicated field geometry exists there: First, there is the radial field. But this alone cannot be the cause, since if this is the only field, the gun works fine. It must thus be the axial field component of the coil that causes the problem. With an axial bias in that region, a quasi-magnetron geometry is obtained. Thus Brillouin clouds can form [38]. Stable electron orbits are greatly enhanced by that and the complex field geometry (X-point, etc.). Breakdown then occurs at the muzzle of the gun, and it is clear that no toroidal current will be measured by the diamagnetical probes. In order to get rid of that problem, a second, much shorter coil with 6 turns having a larger radius than the main coil has been added, as it is shown in Fig. 15. The second coil has opposite current polarity, and has been computed in such a manner that axial field componets cancel out in the very region of the muzzle. The axial and radial componets of the field, into which the plasmoid is injected, are

[9] The breakdown occurs a little after the current goes through zero, so that there is a toroidal magnetic field

shown in Fig. 16 a) and b). It must not be forgotten that those are twisted into a helix by the toroidal field of the central conductor. After having added that second coil, the gun worked just fine, so that the injection could be studied. This sensitivity of the breakdown to axial field components is also of importance to other guns, which are operated with axial bias in the discharge chamber region. Then, the breakdown region is no longer exactly defined, so that operation problems may arise.

4.3. Results of Plasma Diagnostics with Toroidal Bias Field

The optimum parameters within the range of variation are for this case: a discharge potential of 13 kV, and a pressure of 50 mT, which has been computed to be the optimum. The pulses obtained were very highly reproducible, only unsignificant noise levels made up the vanishing difference. Consider fig. 17 - 22. In fig. 17 (data are given in each figure's legend) it is clearly visible, that the plasmoid with the toroidal current moves down the driftspace. The pulse becomes smaller since the current decays, and due to ∇u_z, the pulse widens because the plasmoid is streched. Fig. 18 -22 show the same, but the signals can be viewed much clearlier. Fig. 18 indicates a time delay of 2 µsec between two subsequent probes. Since the probes are spaced 4.8 cm apart from each other, the mean velocity is 2.4 cm/µsec. To compare: The MHD-model from section 2 predicts a velocity of 2.6 cm/µsec (compare with table 3)! The time delay between the second (D2) and the third (D3) diamagnetical probe is measured to 2.5 µsec, thus u_z =1.9 cm/µsec. Again, the model predicts 2.1 cm/µsec! This is really a very good agreement with the experiment. From the fig. 17 - 22 it is clear that the toroidal current lasts for at least 12 µsec; which is rather long. The toroidal plasma current is computed from the extreme value of the pulse. For this probe design it is 2.13 kA/V. Thus the current in the torus is 6.4 kA when passing the first probe, but then it decays rapidly, so that q is expected to increase, generally leading to higher stability. The length of the pulse allows the computation of the length of the elongated torus. It is found that the torus has a length of about 8 cm, which changes slightly as it propagates down the driftspace[10]. The torus is very compact, as in a Spheromak. The magnetical diagnostics confirmed a very homogenous toroidal current, because signals from the 3 coils per plane were identical. No n instabilities were observed, the decay of the current is very continuous and does not happen abruptly. No oscillatory instability occurred. Transverse expansion did indeed not take place, due to the rarefaction wave pattern discussed in section 2.

4.4. Results of Plasma Diagnostics with Helical Bias Field

For this particular design, the optimum parameters within the range of variation are: 13 kV / 50 mT / 1000A coil current, thus B_{max} = 0.065 T, $l_i \cong 1.2$, $\beta_p \cong 0.7$, and $q \cong 3$[11]. This is about three times less than the equilibrium field computed according to Shafranov's formula. The explanation will be given later on, since it is combined with some other effect. Again, the pulses obtained were highly reproducible. The speed of the sheet in the driftspace is only insignificantly affected by the magnetic field. The geometry of the field, into which the torus is injected with $\beta = 0.7$, has been shown in fig. 16. Fig. 23- 26 show what is expected to happen to the plasmoid: the penetration into the stronger helical field region causes the toroidal current to decrease more rapidly. Fig. 27- 31 are the same series as fig. 18 - 22 expect that now, the discussed field geometry exists. Consider fig. 27; the first 15 µsec are noise, then, there is a short positive pulse followed by a wider, negative

---

[10] These calculations are not shown, since they are only of technical nature. For the same reason, the Laplace network analysis is not shown for the discharge current, the axial field coil discharge, or for the diamagnetical probe signal.

[11] The determination of the time-dependence of these parameters is beyond the diagnostical capacity of the apparatus and the scope of the work.

one. This includes a neat diamagnetical measurement of the preceding fast shock wave: When the shock front reaches the muzzle of the gun, helical current discharges take place into the drift space[12]. Those are caused by the ionizing front being ejected, forming a rarefaction wave pattern. The flowing of helical currents has been observed previously by others, in some cases, the helical current had the from of a helical pinch exiting from the central electrode [7]. But in that case, each probe should measure the same time of occurrence of the positive pulse after triggering. And furthermore, in fig. 27 the ratio of the time of occurrence of the pulse amplitudes of the negative and the positive pulse should be $(f+1)/f = 1.33$, since the shock speed equals $(f+1)/f$ times the sheet speed. This is exactly what is observed, in fig. 27 the ratio is 1.3, and throughout fig. 27- 31 the positive pulse occurs at the same time. It is observed that the toroidal current decays more rapidly, because of the penetration into the strong field region. Eventually, the toroidal current seems to be reversed. This is due to the fact that the propagating plasma continues as a homogenously *distributed cylindrical helical current discharge due to the resulting* Lorentz force. If the field polarity were reversed, one expects that the toroidal current, and therefore the flux be amplified[13]. But upon changing the field polarity, the electron cloud effect again took place, so that no toroidal current was measured (because of a bad breakdown). This is also the explanation of why the optimum field is 3 times less than the computed value. According to the computation, the current in the coil should be 3 kA. But then, toroidal current reversal occurs much faster (fig. 32 & 33). And that it was impossible to synchronize in order to achieve flux amplification was just discussed to be due to bad breakdowns. The magnetic diagnostics give the same conclusion as in the previous section: the toroidal current again is very homogenous and decays continuously, not abruptly. No oscillatory instabilities ocurred. If the stabilizing effect of the magnetic field in particular is to be studied, it is better to operate the gun with a gaspuff, since the stabilizing effect of the rarefaction wave pattern is considerable.

4.5. Variation of Parameters

The optimum discharge voltage was determined to be 13 kV. If the potential was risen above that, breakdown occurred right on the beginning of the first half-period, often resulting in much noise and non-reproducible pulses due to inhomogenous breakdowns. When the voltage was reduced to 8 kV, not much plasma mass left the gun, or no plasma discharge took place at all. The pressure was varied within 10 mT to 200 mT, but only in the region of 20 mT to 70 mT a toroidal current was measured. Above 70 mT, breakdown again is affected, so that pulses become much noisier and are less reproducible. Furthermore, the resistance of the plasma becomes higher, so that the toroidal current decays much faster. For the sheet speed the model predicts: $u_z \sim p^{-1/2}$, this was observed and is shown in fig. 34 (consider its legend). The axial magnetic field was varied between 0.065 T and 0.26 T (max. flat-top values). It was observed that the stronger the field the faster the toroidal current was reversed, because of the resulting Lorentz force. Synchronization was impossible to achieve, as discussed in section 4.4. . Fig. 35 shows the timing of the two discharges, whereas fig. 36 shows the discharge current on the same timescale along with the signal from the first diamagnetical probe.

---

[12] A helical current discharge is encountered when helical current exits from the flat end of the inner cylindrical electrode into the driftspace (not the same as the ejected plasmoid or the central conductor leakage current). The experimental setup is in such a way, that the probes must give a positive pulse for a helical current discharge, and a negative one for the propagating toroidal plasma current, because the current polarities are opposite.

[13] Where the energy is supplied from the axial bias field

5. CONCLUSION

A time-dependent MHD current element model for the coaxial plasma gun in the high density regime was derived and examined by the experiment. The very good agreement between experiment and model was shown. It was found that radial motion and thermal diffusion can very well be neglected during the acceleration. The design of the gun used in this experiment was described, and design considerations given. Some modifications, i.e. the central conductor and the aluminum cage, turned out to be rather useful in determining what is happening. The unique design allowed to measure both time delays of the plasmoid and the shock wave with the same array of diamagnetical probes. The stability was enhanced by two factors: (1) toroidal, respectively helical bias field, and (2) by prevention of transverse expansion in the driftspace through the rarefaction wave pattern. The operation of the gun was very much breakdown-characteristics dependent. The findings of the enhanced stability and of the central conductor operation mode should be of interest to further plasma gun research, and to injection devices for magnetic confinement as discussed in the introduction, specially for Spheromaks.

ACKNOWLEDGMENTS

The author is greatly indebted to his mentor Dr.R. Keller for his help and comments. Without him, this work would never have existed. Furthermore, since the author is still secondary student and not permanently working at CRPP, special thanks to the CRPP and everyone there who helped. The work was supported by a very generous grant from ATEL Inc./ Olten. Also, the author would like to thank the teachers it concerns and the principal of the Gymnasium of the Kantonsschule Hardwald for their understanding. Finally, thanks to my parents and the rest of my family for their support.

APPENDIX - FORMULA NOTATION

The selected formula notation is given in the order of appearance:

I	main discharge current	I_0	amplitude of ignition half-period
ω	circuit resonant frequency	t	time
L_x	inductivity of x (for example L_{gun})	r	radius
n	particle density	e	elementary charge
D	diffusion coefficient	μ_0	permeability of vacuum
σ	conductivity	ε_0	permittivity of vacuum
k	Boltzmann constant	T	electron temperature
Z	order of ionisation	m_e	electron mass
M	total mass	u_z	axial velocity; sheet speed
u_r	radial velocity	γ	=(f+2)/f
f	degrees of freedom	u_s	shock front velocity
p_1	pressure in compression-region	ρ_0	mass density of restgas
u	velocity	I_p	toroidal plasma current
κ	apparent flux conservation factor	Φ	permanent flux
a	plasma minor radius	R	plasma major radius
b	distance aluminum cage - R	t_0	ejection time of a certain inf. elem.
l_{gun}	length of the gun	u_0	axial speed at ejection
B_a	axial bias field strength	q	safety factor
β_p	confinement efficiency	l_i	internal inductance
B_θ	poloidal magn. field strength	B_ϕ	toroidal magn. field strength

REFERENCES

[1] J. Marshall; "ACCELERATION OF PLASMA INTO VACUUM"; in *Proceedings of the Second United Nations Conference on the Peaceful Uses of Atomic Energy*; United Nations, Geneva, Vol. 31, pp. 341-347, 1958

[2] H. Alfvén; "MAGNETOHYDRODYNAMICS AND THE THERMONUCLEAR PROBLEM"; in *Proceedings of the Second United Nations Conference on the Peaceful Uses of Atomic Energy*; United Nations, Geneva, Vol. 31, pp. 3-5, 1958

[3] J. Marshall; "PERFORMANCE OF A HYDROMAGNETIC PLASMA GUN"; Phys. Fluids, Vol. 3, N. 1, pp. 134-135, Jan. 1960

[4] H. Alfvén, L. Lindberg, P. Mitlid; "EXPERIMENTS WITH PLASMA RINGS"; J. Nucl. Energy C, Vol. 1, pp. 116-120, 1960

[5] C.T. Chang; "SHOCK WAVE PHENOMENA IN COAXIAL PLASMA GUNS"; Phys. Fluids, Vol. 4, N. 9, pp. 1085-1096, Sep. 1961

[6] D.M. Wetstone; "COAXIAL PLASMOID SOURCE OF SMALL ASPECT RATIO"; Phys. Fluids, Vol. 5, N. 8, pp. 981-987, Aug. 1962

[7] L. Lindberg, C.T. Jacobsen; "STUDIES OF PLASMA EXPELLED FROM A COAXIAL PLASMA GUN"; Phys. Fluids Supp. 1964, Vol. 7, N. 11, pp. S44-S50

[8] J.W. Mather; "INVESTIGATION OF THE HIGH ENERGY ACCELERATION MODE IN THE COAXIAL GUN"; Phys. Fluids Supp. 1964, Vol. 7, N. 11, pp. S28-S34

[9] D.M. Wetstone, I. Greber; "AZIMUTHAL PLASMOID MOTION IN A COAXIAL SOURCE WITH B_Z BIAS FIELD"; Phys. Fluids Supp. 1964, Vol. 7, N. 11, pp. S35-S40

[10] C.J. Michels, P. Ramins; "PERFORMANCE OF COAXIAL PLASMA GUN WITH VARIOUS PROPELLANTS"; Phys. Fluids Supp. 1964, Vol. 7, N. 11, pp. S71-S74

[11] G. Hergizer, H. Krompholz, W. Schneider, K. Schönbach; "A STEADY-STATE FLUID MODEL OF THE COAXIAL PLASMA GUN"; Phys. Lett., Vol. 71A, N. 1, pp. 54-56, Apr. 1979

[12] Yu.V. Skvortsov; "RESEARCH ON PULSED AND STEADY-STATE PLASMA GUNS AND THEIR APPLICATIONS IN THE TROITSK BRANCH OF KURCHATOV INSTITUTE OF ATOMIC ENERGY"; Phys. Fluids B, Vol. 4, N. 3, Mar. 1992

[13] D. Dietz; "COAXIAL PLASMA ACCELERATOR IN THE SNOWPLOW MODE: ANALYTICAL SOLUTION IN THE WEAK COUPLING LIMIT"; J. Appl. Phys., Vol. 62, pp. 2669-2674, Oct. 1987

[14] P.K. Browning, G. Cunningham, *et al.*; "INJECTION AND SUSTAINMENT OF PLASMA IN A PREEXISTING TOROIDAL FIELD USING A COAXIAL HELICITY SOURCE"; Phys. Rev. Lett., Vol. 68, N. 11, pp. 1722-1725, Mar. 1992

[15] D.G. Swanson, R.W. Clark, P. Korn, S. Robertson, C.B. Wharton; Phys. Rev. Lett., Vol. 28, p. 1015-, 1972

[16] D.C. Hagerman, J.E. Osher; "INJECTION AND TRAPPING OF β =1 PLASMA INTO A CUSPED MAGNETIC FIELD"; *Phys. Fluids*, Vol. 4, N. 7, Jul. 1961

[17] T.K. Fowler, F.H. Coensgen; "PROGRESS IN MIRROR MACHINE RESEARCH"; in *T.K. Fowler - Mirror Machine Research*; pp. 299-308

[18] R.A. Dory, D.W. Kerst, *et al.*; *Phys. Fluids*, Vol. 9, pp. 997-, 1966

[19] A.W. Leonard, R.N. Dexter, J.C. Sprott; Phys. Fluids, Vol. 30, pp. 2877-, 1987
[20] D.J. Hoffman, J.N. Talmadge, J.L. Shohet; Nucl. Fusion, Vol. 21, pp. 1130-, 1981
[21] P.K. Browning, G. Cunningham, et al.; "THE OPERATION OF THE SPHEROMAK SPHEX WITH A CENTRAL CONDUCTOR"; in *Physics of Alternative Confinement Schemes*, ISPP-8 "Piero Caldirola", S. Ortolani / E. Sindoni (Eds.), SIF / Bologna 1991, pp. 1047-1054
[22] J. Marshall, T.F. Stratton; "THE COLLISION OF TWO PLASMAS"; Nucl. Fusion Supp. 1962, Part 2, pp. 663-674
[23] N.H. Kemp, H.E. Petschek; "THEORY OF THE FLOW IN THE MAGNETIC ANNULAR SHOCK TUBE"; Phys. Fluids, Vol. 2, N. 6, pp. 599-608, Nov. 1959
[24] Mei-Yu Wang, C.K. Choi, F.B. Mead Jr.; "EFFECT OF SPIN-POLARIZED D- /SUP 3/HE FUEL ON DENSE PLASMA FOCUS FOR SPACE PROPULSION"; *AIP Conference Proceedings*, N. 246, pt. 1, pp. 30-34, 1992
[25] T. Ikehata, K. Oohashi, et al.; "PLASMA CENTRIFUGE FOR SEPARATION OF METAL ELEMENTS AND ISOTOPES"; J. Nucl. Instr. & Methods in Phys. Res. B, Vol. B70, N. 1-4, pp. 26-32, Aug. 1992
[26] C. Kim, D.F. Oglatree; "PREPARATION OF MONOLAYERS OF RE AND PT ON METAL SUBSTRATES USING A PULSED METAL PLASMA DEPOSITION SOURCE"; Appl. Surface. Sci., Vol. 59, N. 3-4, pp. 261-266, Jul. 1992
[27] S.K. Iyyengar, V.K. Rohatgi; "CHARACTERIZATION OF A MARSHALL-GUN PRODUCED PLASMA FOR REB-PLASMA INTERACTION"; in *1989 International Conference on Plasma Physics*, Vol. 3, pp. 1165-1168
[28] K.H. Kwek, T.Y. Tou, S. Lee; "CURRENT SHEATH STRUCTURES IN THE RUNDOWN PHASE OF A PLASMA FOCUS"; IEEE Trans. Plasma Sci.; Vol. 18, pp. 826-830, Oct. 1990
[29] M. Rosenbluth, R. Garwin, A. Rosenbluth; *U.S. Atomic Energy Comission*, Report LA-1850, 1954
[30] J. Keck; "CURRENT SPEED IN A MAGNETIC ANNULAR SHOCK TUBE"; Phys. Fluids Supp. 1964, Vol. 7, N. 11, pp. S16-S27
[31] L.C. Burkhardt, R.H Loveberg; "CURRENT SHEET IN A COAXIAL PLASMA GUN"; Phys. Fluids, Vol. 5, N. 3, pp. 341-347, Mar. 1962
[32] D.J. Rose, M. Clark Jr.; "PLASMAS AND CONTROLLED FUSION"; M.I.T. Press 1961
[33] L. Spitzer; "PHYSICS OF FULLY IONIZED GASES"; Interscience Publishers, INC., New York, 1956
[34] R. Courant, K.O. Friedrichs; "SUPERSONIC FLOW AND SHOCK WAVES"; Interscience Publishers, INC., New York, 1961
[35] K. Thorn, J. Norwood, N. Jalufka; "VELOCITY LIMITATION OF A COAXIAL PLASMA GUN"; Phys. Fluids Supp. 1964, Vol. 7, N. 11, pp. S67-S70
[36] V.D. Shafranov, V.S. Mukhovatov; "PLASMA EQUILIBRIUM IN A TOKAMAK"; Nucl. Fusion, Vol. 11, pp. 605-633, 1971
[37] J. Wesson; "TOKAMAKS"; *Oxford Engineering Science Series - 20*, Clarendon Press, 1987
[38] Om P. Gandhi; "MICROWAVE ENGINEERING AND APPLICATIONS"; Pergamon Press, 1986

FIGURE CAPTIONS

Fig. 1: Current sheet and shock region in the coaxial plasma gun.
Fig. 2: Current sheet at the muzzle of the gun.
Fig. 3: Ejected current-carrying (elongated) plasmatorus in the driftspace.
Fig. 4: Illustration of an infinitesimal current sheet element.
Fig. 5: Discharge current distribution geometry.
Fig. 6: Graph of z(t); from t=2μsec on z increases almost linearly with t. Ejection is at z=15 cm, which is the length of the gun. Then t=5μsec. Of course, the graph is no longer valid for t>5μsec for this gun, but to illustrate that the curve is almost this section was included too. It would hold for a gun with longer electrodes, i.e. larger ejection time.
Fig. 7: Graph of $u_z(t)$; it is seen that the maximum speed of 4.5cm/μsec is reached at approx. t=3.2μsec. At ejection u_z=3.5cm/μsec.
Fig. 8: Motion of the plasmoid in the acceleration phase computed according to (16,17).
Fig. 9: Simplified rarefaction-wave pattern at the muzzle preventing significant transverse expansion. The intercepting shock wave pattern was simplified.
Fig. 10: Same as fig. 6, but for the driftspace phase. The function is still close to be linear within the relevant times. Here, t=0 and z=0 at ejection.
Fig. 11: Same as fig.7, with the same modification as in fig. 10.
Fig. 12: Heartpiece of the apparatus: 1 - inner electrode/ 2 - outter electrode/ 3 - ignition aid (INOX disc)/ 4 - central conductor/ 5 - thin pyrex tube insulating the central conductor/ 6 - pyrex tube of the driftspace/ 7 - aluminum cage/ 8 - driftspace/ 9 - teflon disc/ 10 - coil spring/ 11 - copper cross, together with 9,10 fixing 5 elastically/ 12 - removable bottom plate/ 13 - fixed bottom plate/ 14 - permanent flux guide (not constucted in axial symmetry)/ 15 - teflon insulation layer/ 16 - permanent magnet/ 17 - teflon ring insulating the two discharge electrodes/ 18 - O-ring/ 19 - neoprene ring for elastic fixation of 6/ 20 - hexagonal cage fixing axial field coil and the probes of the diagnostics/ 21 - muzzle.
Fig. 13: Array of probes and one diamagnetical probe consisting of two nested loops in detail.

Fig. 14: Typical oscillogram for the discharge current (channel 1) and the current in the central conductor (channel 2). Channel 1: 4.3 kA/V/ Channel 2: 2.5 kA/V. The vertical spike at t=15μsec indicates breakdown. The first half period is longer since the discharge current flows through the central conductor loop, which has a much higher inductivity.

Fig. 15: Axial field coil with opposite current polarity compensation coil.

Fig. 16: Axial and radial components of the magnetic field, into which the plasmoid is injected. This geometry is actually twisted into a helix by the azimuthal components of the field. In the case of +4000 A (a) the gun worked fine, but for opposite field polarity (-4000 A) (b) in order to achieve flux amplification no toroidal current was measured. The bad breakdown for the latter situation is also influenced by the clearly visible X-point (-4000 A). The permanent field was represented with a current carrying loop. Not all field lines are shown for clarity.

Fig. 17: The movement of the torus in the driftspace can easily be viewed in this picture from the oscilloscope. From top trace to bottom trace: D1 (2V/div), D2 (2V/div), D3 (1V/div), D4 (.5V/div), where D means diamagnetical probe and the higher the index the farther away the probe is from the muzzle. 5μsec/div; p=50mT; 13kV discharge potential.

Fig. 18: The same parameters as in fig. 17: Channel 1: D1/ Channel 2: D2

Fig. 19: Analogously to fig. 18.

Fig. 20: Analogously to fig. 18.

Fig. 21: Analogously to fig. 18.

Fig. 22: Analogously to fig. 18.

Fig. 23: Radial and axial field components after injection. The moving plasmatorus is approximated with a current carrying loop. For this figure, the axial coil discharge current was 1000 A and the current in the ring 5000 A with opposite polarity. Note that this is only a model. Behind the plasma, a X-point occurs. The positions of the turns of the coils are clearly visible. The muzzle is at z=0 between r=3 cm and r=5 cm. The axis is at r=0.

Fig. 24: Cont. fig. 23.

Fig. 25: Cont. fig. 24.

Fig. 26: Cont. fig. 25.

Fig. 27: The same series as fig. 18-22, but for helical bias field. The notation is still the same as in fig. 18-22. The explanation of the fig. is given in the text.

Fig. 28: Analogously to fig. 27.

Fig. 29: Analogously to fig. 27.

Fig. 30: Analogously to fig. 27.

Fig. 31: Analogously to fig. 27.

Fig. 32: The notation is still the same; the axial field discharge current is here +4000A. First there seems to be no difference to fig. 27.

Fig. 33: Already at D3 the toroidal current is zero and will be reversed in the following.

Fig. 34: Pictrure from the oscilloscope; from top to bottom trace: D1,D2 (60mT) / D1,D2 (40mT), where the deflection is .2V/div; 5μsec/div, 12kV. According to the model, the ratio of the two time delays should be 0.81, to which the measured ration of 0.78 is in agreement.

Fig. 35: Timing of the two discharges. Upper trace: plasma discharge current/ Lower trace: axial field coil discharge current. The sensitivities of the traces have been selected in such a way that the signals can be viewed clearly.

Fig. 36: Plasma discharge current and signal of D1. Upper trace D1 (.5V/div)/ Lower trace: plasma discharge current (uncalibrated). 5μsec/div / 60mT / 12kV. The first half-period is longer since the current flows through the central conductor.

PHOTOGRAPHS

Picture 1: Total view of the apparatus at the CRPP.

Picture 2: Heartpiece, i.e. coaxial plasma gun at an early experimental stage.

Picture 3: Rak with diagnostics and discharge triggering system.

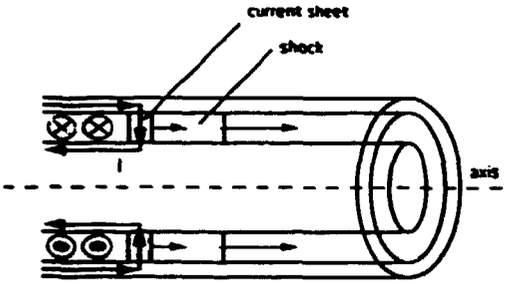

Fig. 1

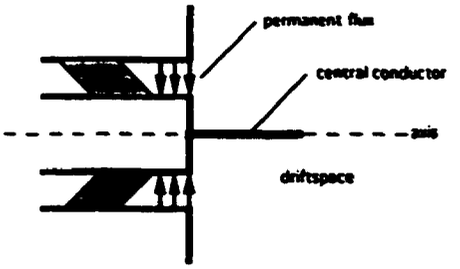

Fig. 2

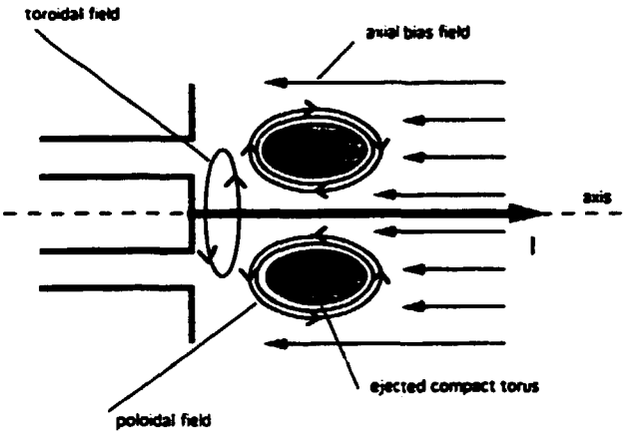

Fig. 3

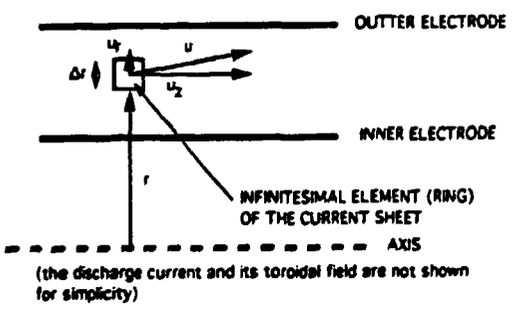

Fig. 4

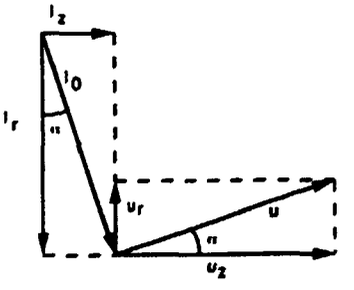

Fig. 5

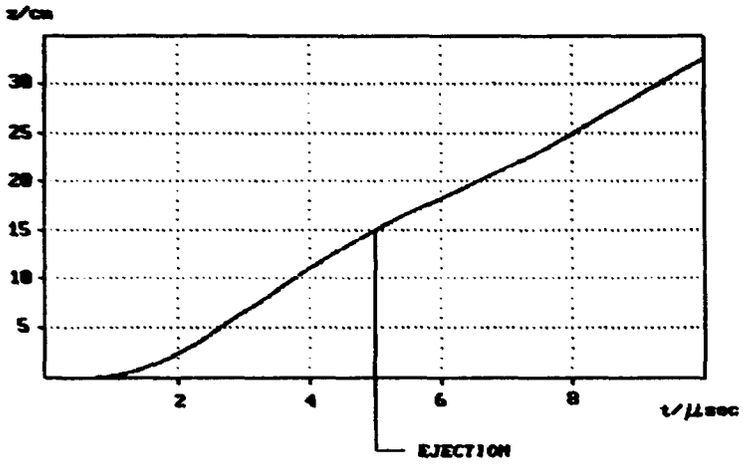

Fig. 6

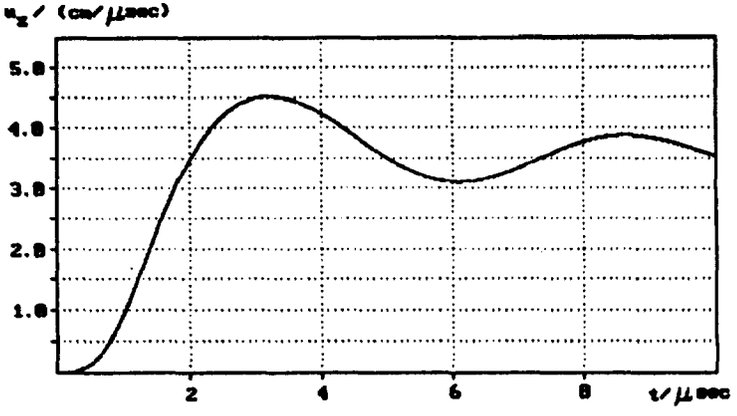

Fig. 7

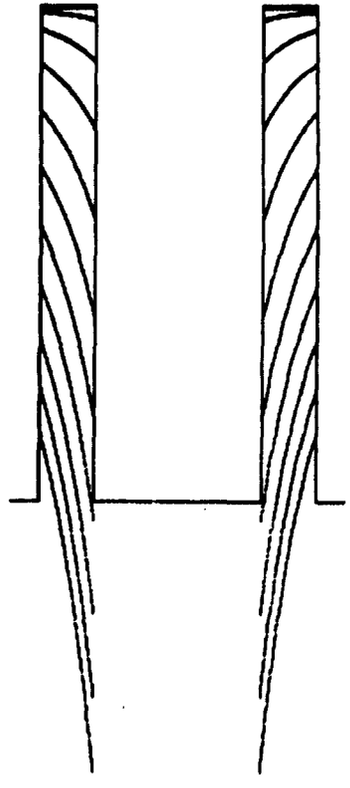

Fig.8

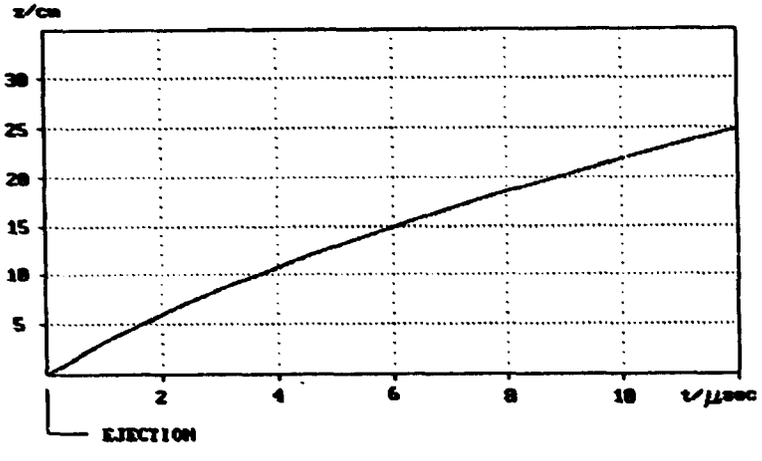

Fig. 10

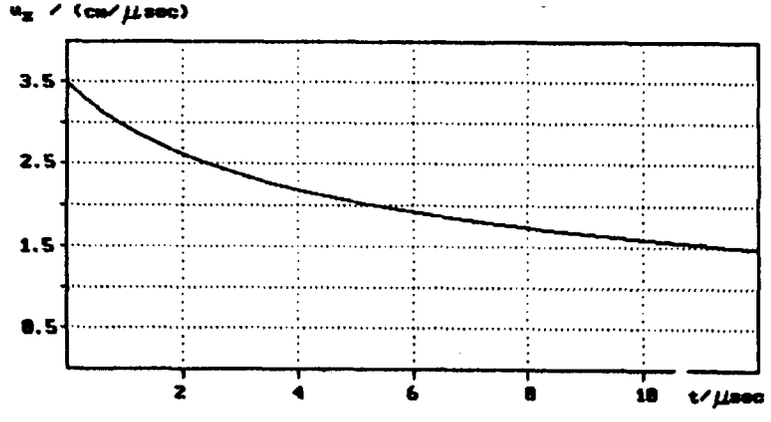

Fig. 11

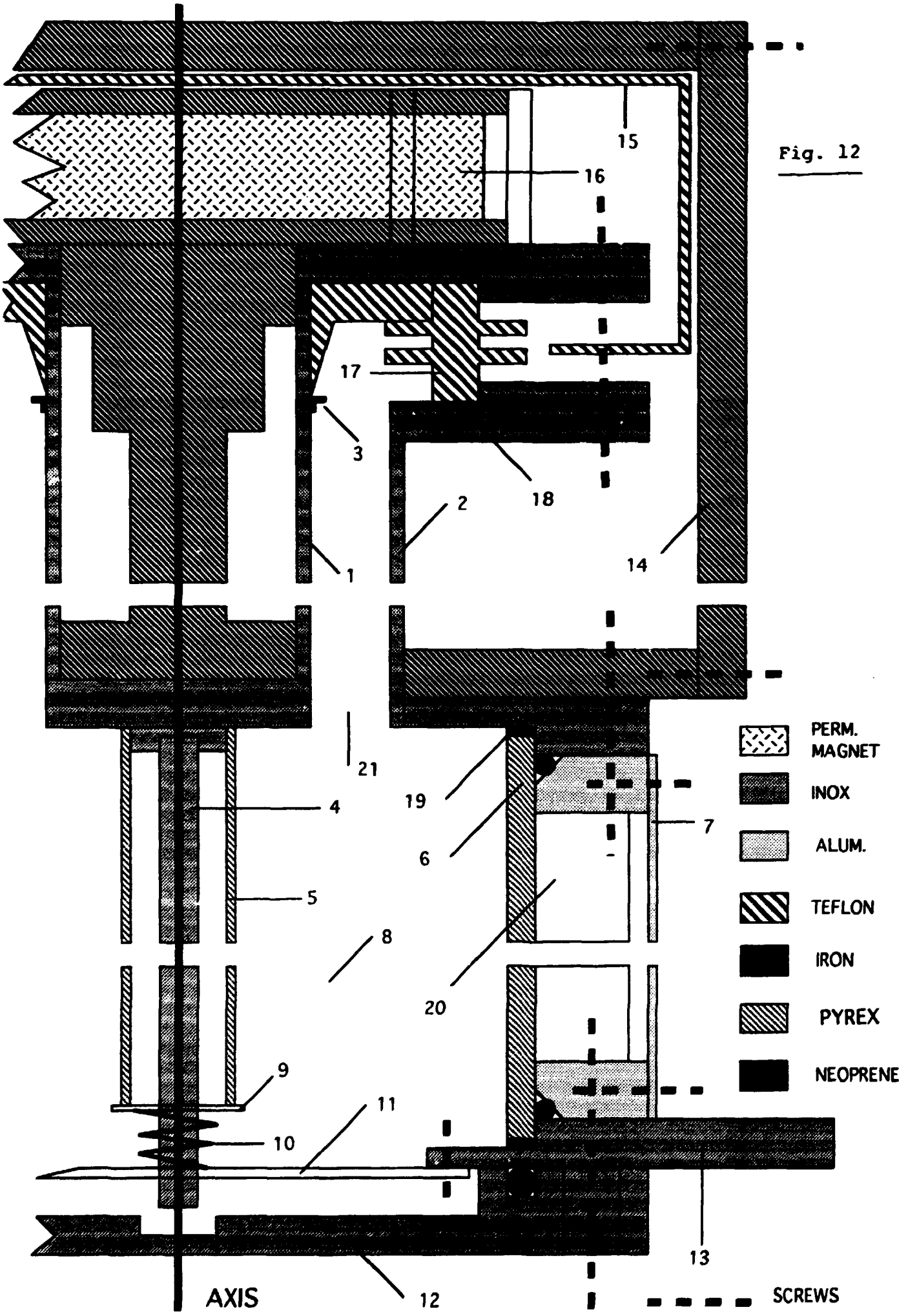
15
16
17
3
18
2
1
14
21
19
4
6
7
5
8
20
9
11
10
13
12
AXIS
SCREWS
PERM. MAGNET
INOX
ALUM.
TEFLON
IRON
PYREX
NEOPRENE

Fig. 12

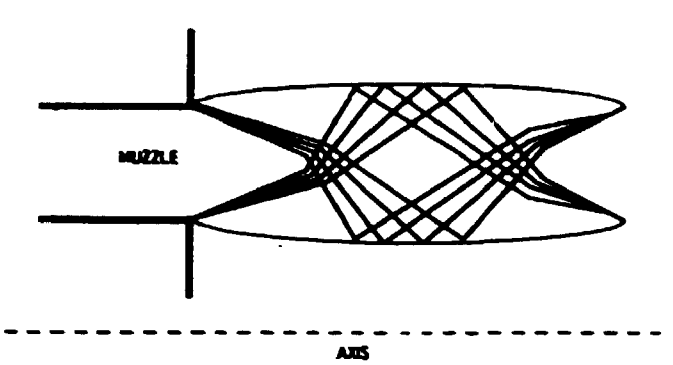

Fig. 9

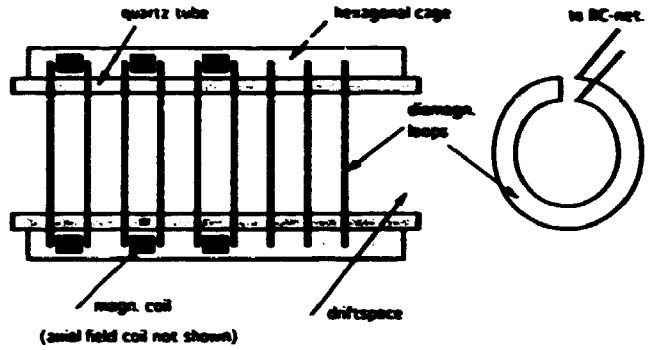

Fig. 13

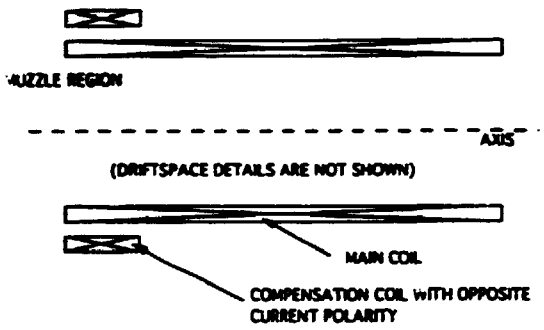

Fig. 15

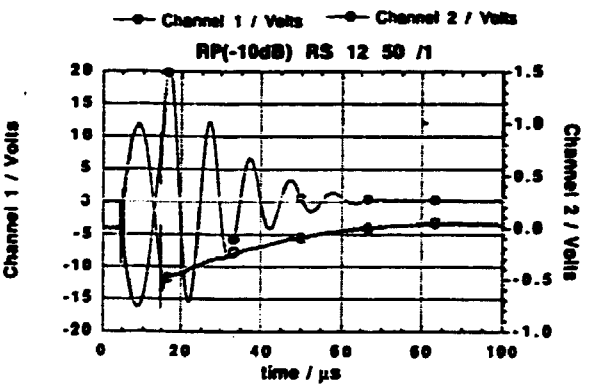

Fig. 14

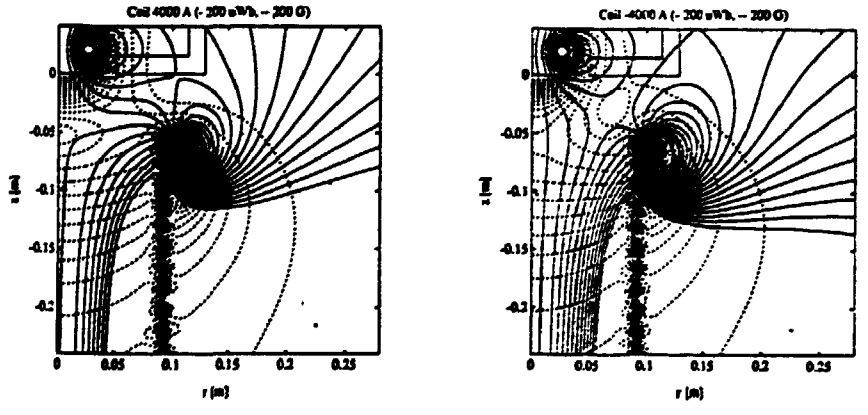

a) b)

Fig. 16

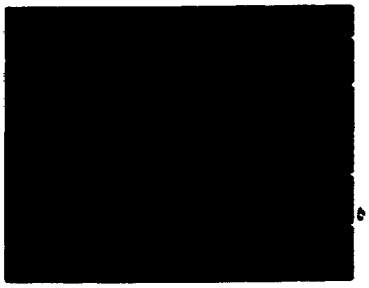

Fig. 17

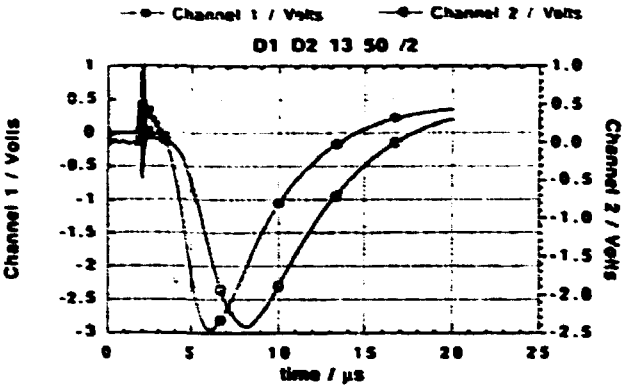

Fig. 18

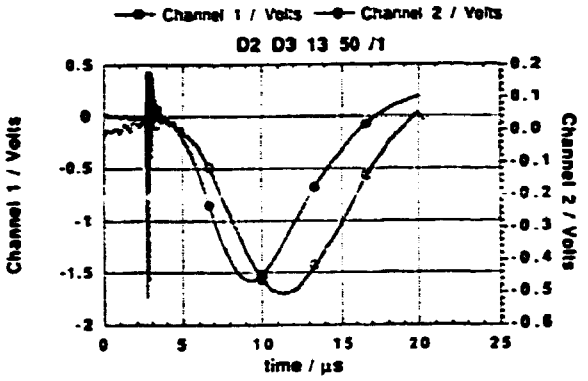

Fig. 19

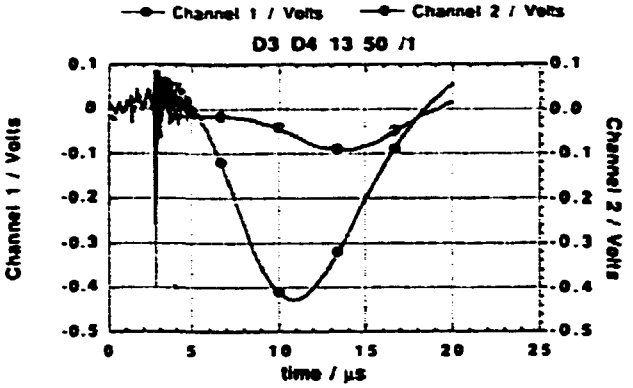

Fig. 20

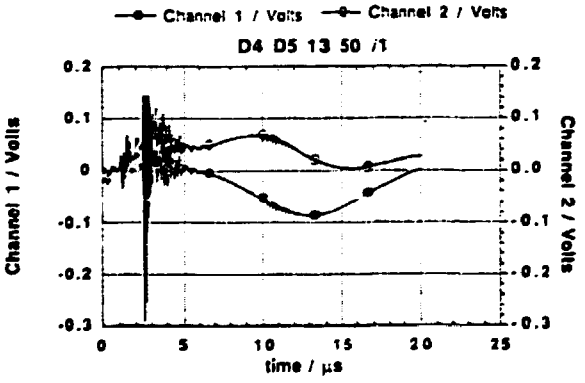

Fig. 21

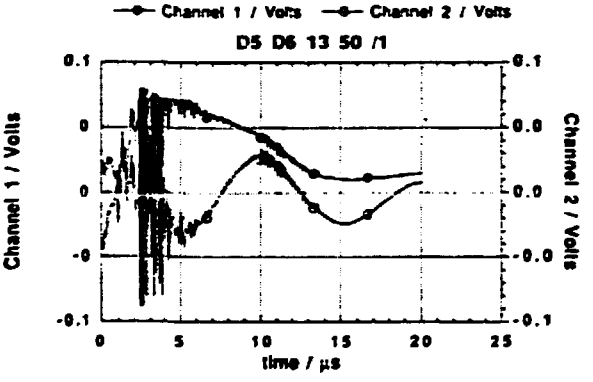

Fig. 22

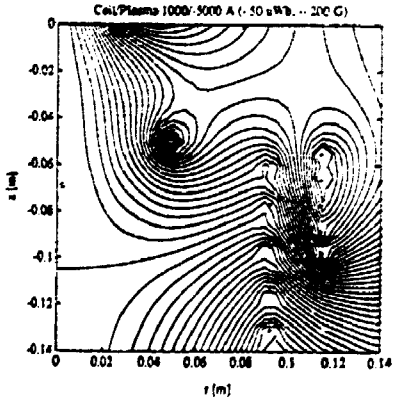

Fig. 23

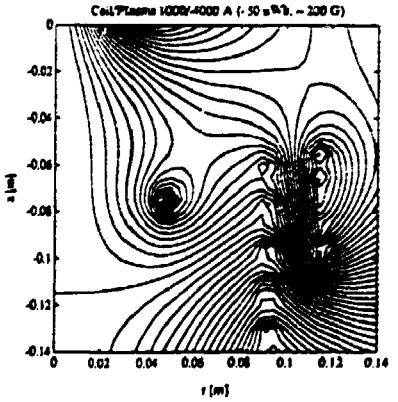

Fig. 24

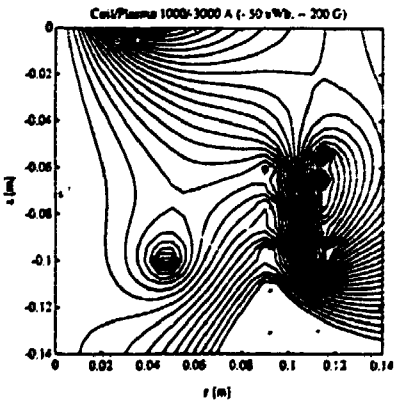

Fig. 25

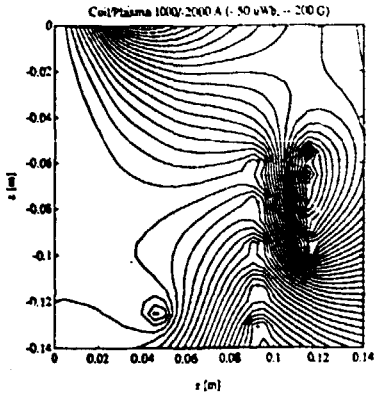

Fig. 26

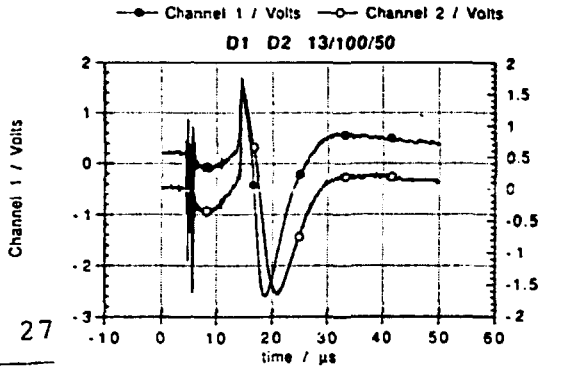

Fig. 27

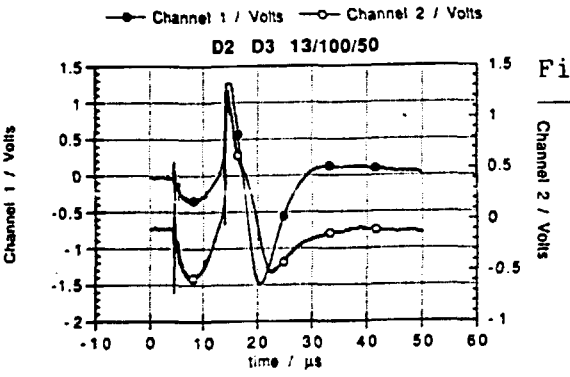

Fig. 28

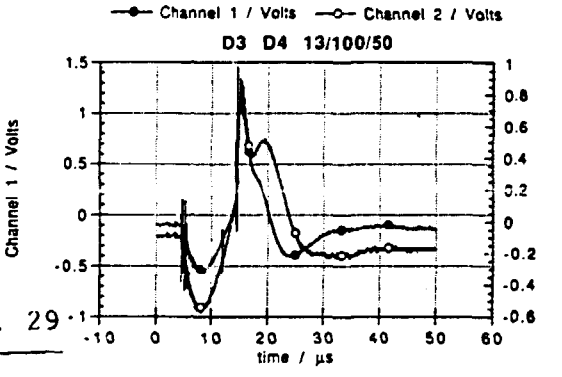

Fig. 29

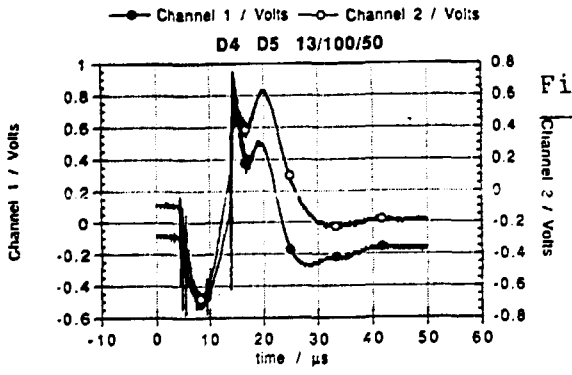

Fig. 30

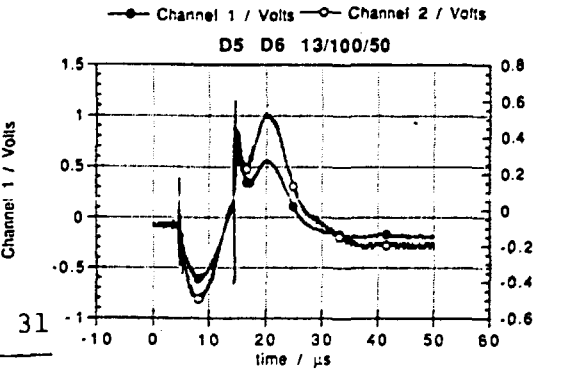

Fig. 31

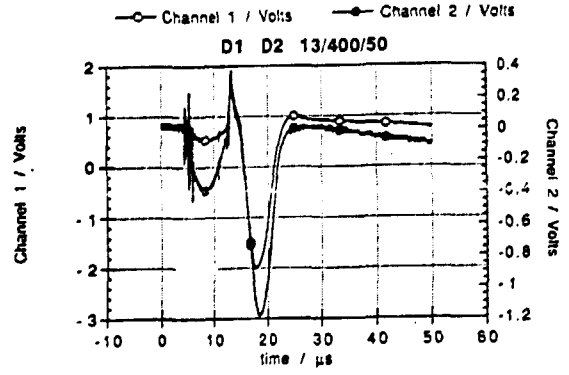

Fig. 32

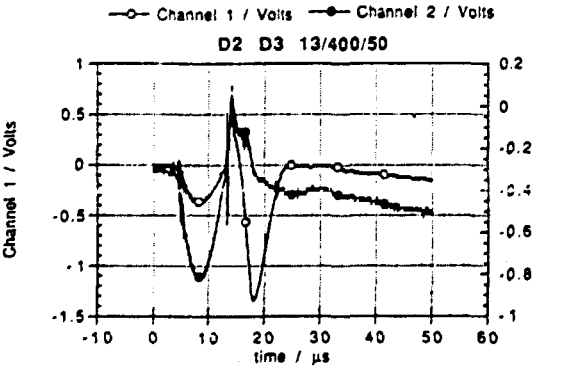

Fig. 33

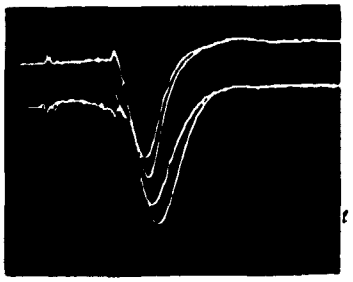

Fig. 34

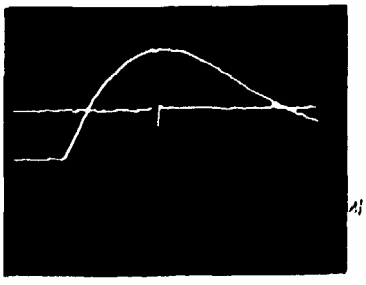

Fig. 35

Fig. 36

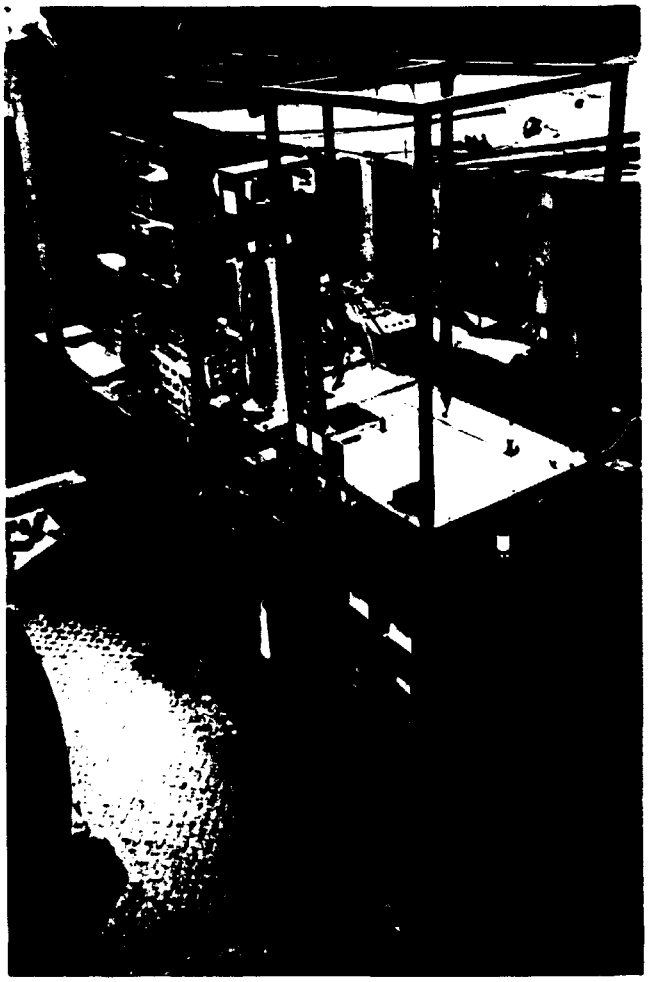

Pict. 1

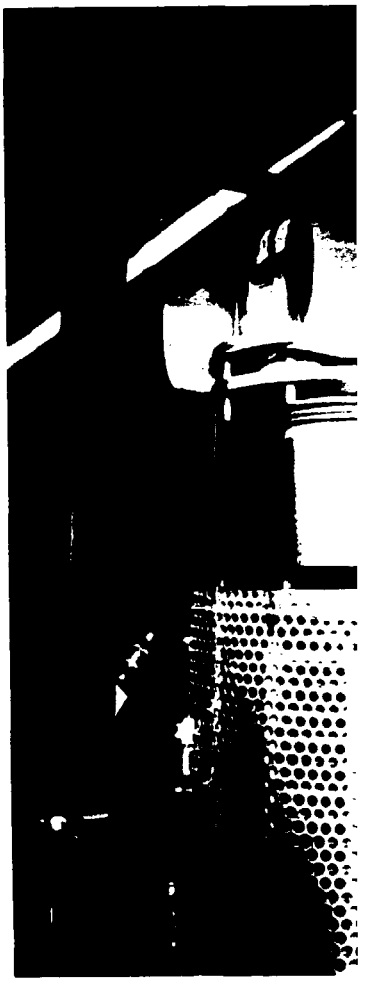

Pict. 2

Pict. 3